Applied Surface Science 439 (2018) 1010–1018

Contents lists available at ScienceDirect

Applied Surface Science

journal homepage: www.elsevier.com/locate/apsusc

Full Length Article

Effect of Ga incorporation on morphology and defect structures evolution in VLS grown 1D In_2O_3 nanostructures

Jesús Alberto Ramos-Ramón [a], Umapada Pal [a,*], Ana Cremades [b], David Maestre [b]

[a] Instituto de Física, Benemérita Universidad Autónoma de Puebla, Apdo. Postal J-48, Puebla Pue. 72570, Mexico
[b] Departamento de Física de Materiales, Facultad de Ciencias Físicas, Universidad Complutense de Madrid, 28040 Madrid, Spain

ARTICLE INFO

Article history:
Received 10 October 2017
Revised 9 January 2018
Accepted 13 January 2018
Available online 17 January 2018

Keywords:
Indium oxide
Vapor-liquid-solid
Controlled growth
Defect structure
Cathodoluminescence

ABSTRACT

Fabrication of 1D metal oxide nanostructures of controlled morphology and defect structure is of immense importance for their application in optoelectronics. While the morphology of these nanostructures depends primarily on growth parameters utilized in physical deposition processes, incorporation of foreign elements or dopants not only affects their morphology, but also affects their crystallinity and defect structure, which are the most important parameters for their device applications. Herein we report on the growth of highly crystalline 1D In_2O_3 nanostructures through vapor-liquid-solid process at relatively low temperature, and the effect of Ga incorporation on their morphology and defect structures. Through electron microscopy, Raman spectroscopy and cathodoluminescence spectroscopy techniques, we demonstrate that incorporation of Ga in In_2O_3 nanostructures not only strongly affects their morphology, but also generates new defect levels in the band gap of In_2O_3, shifting the overall emission of the nanostructures towards visible spectral range.

1. Introduction

Metal oxide based semiconductors such as ZnO, SnO_2, In_2O_3, TiO_2 and Ga_2O_3 received enormous attention in recent time, especially for their applications in catalysis [1], fabrication of solar cells [2], gas sensors [3], field-effect transistors [4], and photodetectors [5]. For these applications, In_2O_3 has been one of the most utilized materials due to its adequate optical and electrical properties. Being a wide-band-gap semiconductor (~3.6 eV) with high optical transmittance [3], good electrical conductivity [6], and high chemical stability [7], In_2O_3 is considered as a very important material for optoelectronic applications [8], especially in nanostructure forms. For instance, nanostructured In_2O_3 presents intense luminescent emission in the UV–visible range [9], leading its application in LEDs (*light-emitting diodes*). However, fabricating nanostructures with specific morphologies is an important task for manipulating their physical properties required for specific application. In order to tune their physical properties, In_2O_3 nanostructures have been grown with different morphologies such as octahedral particles [10], rods [11], wires [12], and doped with different elements like Sn [13], Zn [14], and Ga [10,15]. Effects of morphology and doping on their optical and optoelectronic properties have also been studied. Incorporation of foreign elements can induce changes in microstrain, modifying crystallite size of In_2O_3 nanostructures [10]. The microstrain in In_2O_3 lattice depends on the difference between the ionic radii of In and the dopant ion. However, it has been demonstrated that Ga incorporation in indium oxide octahedral nanoparticles fabricated by vapor–solid (VS) method does not affect significantly their crystallinity due to the isovalent substitution of In^{3+} ions by Ga^{3+} ions [10]. When the dopant element has different valence charge than indium, the formation of oxygen-related defects through charge compensation might be induced. Formation of such defects modifies the physical properties such as electrical conductivity, which is typically related to oxygen vacancies (V_O) in metal oxide semiconductors. It is well known that Sn-doped indium oxide systems (also called ITO) have enhanced electrical conductivity in comparison with pristine indium oxide, which makes them suitable for transparent contact applications in solar cells. However, the typical sheet resistance of 10 Ω/square is inadequate for applications in flat panel displays. Although by increasing thickness, the sheet resistance of ITO films can be reduced, it leads to undesirable increment in the optical absorption of the films. Moreover, their high absorption in the near infrared region (1.0–1.5 μm) is an issue that the scientific community has tried to solve. In order to overcome this situation, Ga- and Zn-doped thin films have been developed, which have proved to be good substitutes of In in transparent conducing oxide (TCO) thin

* Corresponding author.
E-mail address: upal@ifuap.buap.mx (U. Pal).

https://doi.org/10.1016/j.apsusc.2018.01.125
0169-4332/

films due to less optical absorption in the near infrared region with electrical conductivity similar to Sn-doped systems [14,16]. On the other hand, Zn-doped indium oxide nanostructures have been applied in the fabrication of field-effect transistors (FETs) with conductivity values similar to Sn-doped indium oxide based FETs [17]. The optical properties such as luminescence emissions of indium oxide depend strongly on the fabrication method and the nature of dopant element. Gao *et al.* [18] found that the photoluminescence emissions of ITO nanowires synthesized by VLS process shift from visible (1.9 eV) to UV (~2.9 eV) region on the increase of Sn fraction. Despite the abundance of literature reports on the effect of dopant incorporation on their physical properties of In_2O_3 nanostructures, there exist no clear picture due to the involvement of a vast number of parameters, especially in the used physical growth techniques.

In the present work, we report on the fabrication of Ga-incorporated In_2O_3 nanostructures of different Ga contents by a simple, solvent-free vapor-liquid-solid (VLS) method at relatively low temperature. The effects of Ga incorporation on the morphology, crystallinity, optical behavior, electronic defect structures and photocatalytic degradation performance on methylene blue (MB) dye of indium oxide nanostructures are discussed highlighting their potentialities for optoelectronic applications.

2. Materials and methods

In_2O_3 nanostructures were fabricated through VLS process, utilizing a horizontal tube furnace with multiple gas supply facility. Metallic indium droplets (~2 mm, 99.9% purity, Sigma-Aldrich), graphite powder and metallic gallium splatter (99.99% purity, Sigma–Aldrich) were put in a quartz crucible with a 1:0.6:X (X = 0, 0.05, 0.10 and 0.20, defined as sample GIO-0, GIO-5, GIO-10 and GIO-20, respectively) nominal weight ratio. Silicon substrates (1.5 cm × 2.0 cm) covered with a ~15 nm thick sputtered deposited Au film were set face-down over the quartz crucible, with a distance of ~7 mm separating the precursors and the substrate. The precursor and substrate loaded crucible was placed at the center of the quartz tube (20 mm internal diameter) of the horizontal furnace and heated to 900 °C at a rate of 37 °C/min, under constant Ar (99.996% purity) + O_2 (99.999% purity) mixture flow (10:1 v/v, 66 sccm). Prior to heating, the growth chamber (quartz tube) was flushed with high purity Ar for 1 h to remove residual air. The growth process was continued for 15 min, after which, the furnace was cooled down to room temperature naturally. For the characterization of the nanostructures, obtained products were gently scratched out from the substrate and deposited over fresh Si substrates. Morphology and elemental composition of the as-prepared nanostructures were analyzed in a Leica Stereoscan 440 scanning electron microscope attached with a Bruker AXS XFlash 4010 X-ray microanalysis (EDS) system. Room temperature cathodoluminescence (CL) spectra of the samples were recorded in a Hitachi S-2500 microscope, utilizing a Hamamatsu PMA-11 charged-coupled device (CCD). MicroRaman spectra of the nanostructures were recorded in a Horiba Jobin Yvon LabRAM HR800 system at room temperature, utilizing a 632.8 nm He-Ne laser and a thermoelectrically cooled CCD. Room temperature UV–Vis absorption spectra of the samples were recorded on their ethanolic colloidal dispersion (0.4 mg of nanostructures dispersed in 2.0 ml of ethanol) using a Shimadzu UV–VIS-NIR 3100PC double-beam spectrophotometer, utilizing pure ethanol as reference. To analyze the structural phase of the nanostructures, X-ray diffraction (XRD) and transmission electron microscopy (TEM) measurements were carried out in a Panalytical XPERT-MPD diffractometer (Cu Kα, λ = 1.54056 Å) and a JEOL JEM 2100 microscope operating at 200 kV, respectively. The chemical states of the elements were determined from the X-ray photoelectron spectra recorded in a Thermo Scientific X-ray photoelectron spectrometer, utilizing Al Kα X-ray source (1486.6 eV). Binding energy of each of the elements was calibrated using C *1s* energy position at 284.6 eV. Photocatalytic performances of the In_2O_3 and Ga incorporated In_2O_3 nanostructures have been tested for methylene blue (MB) degradation under visible and ultraviolet irradiation following the procedure reported in our previous work [19]. Typically, 3 mg of the nanostructures (scratched out from Si substrate) was added into 6 ml of dye solution (10 ppm) under magnetic stirring and air flow in dark (inside a black box). The mixture was left in dark for 60 min under stirring at room temperature (22 °C) to reach the adsorption–desorption equilibrium at the surface of the catalyst. The extent of dye adsorption was determined from the decrease of MB concentration in the solution by monitoring the intensity of its principal absorption band (664 nm) in a Shimadzu UV–VIS-NIR 3100PC spectrophotometer. At different intervals of time, about 2 ml of aliquot was withdrawn from of the mixture to record its absorption spectrum. Once the dye adsorption–desorption equilibrium is reached, the mixture was illuminated either by a UV laser-diode array (365 nm, 10 W) or by a 10 W xenon lamp, emitting white light and the concentration of MB in the mixture was monitored at different intervals by recording its absorption spectra.

3. Results and discussion

SEM images of the samples (Fig. 1) and amplified images of selected nanostructures (insets) revealed the formation of tapered-end rod-like 1D structures of 0.7–2.0 μm length and 20–150 nm width, frequently folded to form elbow-like structures for the sample GIO-0 (Fig. 1a). The presence of quasi-spherical catalyst (Au) particles at the tips of the 1D structures confirms their growth through VLS process. Most of the rods are tapered because of lateral growth of indium oxide through vapor–solid (VS) process and differences in growth time of the bottom ends with respect to their tips [11]. Formation of larger 1D nanostructures (1–5 μm in length and 20–200 nm width) can be observed for the sample GIO-5 (Fig. 1b) containing a nominal 5% Ga. Some of these nanostructures present secondary growths perpendicular to the main structures, and a change in the growth direction, forming elbow-like or kinked structures. In general, the nanostructures have square-like cross-sections, although some of the nanostructures have octagonal cross-sections. On the other hand, 1D structures of 2.7–7.0 μm in length and 200–500 nm width, with square and octagonal cross-sections were formed in the sample GIO-10 (Fig. 1c). While most of the nanostructures have tapered end, structures with thinner ends tend to bend to form curved structures. Although the nanostructures of GIO-0 and GIO-5 samples are frequently branched and contain gold particles at their tips, confirming their growth through VLS process, the nanostructures of sample GIO-10 are usually not branched or elbow-shaped. Finally, the GIO-20 sample revealed the formation of longer nanostructures of higher aspect ratios with tens of microns in length and 45–65 nm in width, without forming tapered ends (Fig. 1d). The sharp increase in the aspect ratio and the formation of tapering-free ends in these nanostructures are due to the incorporation of gallium in indium oxide nanostructures. Ga incorporation is reported to increase the root mean square microstrain, and lattice defects in In_2O_3 lattice, reducing the crystallite size of In_2O_3 structures gradually with increasing Ga content [20]. Formation of longer nanostructures in this sample clearly indicates an enhancement in growth rate due to the incorporation of Ga in In_2O_3 nanostructures. High growth rate of these nanostructures not only ceases the formation of tapered ends, also leads to the formation of longer rods.

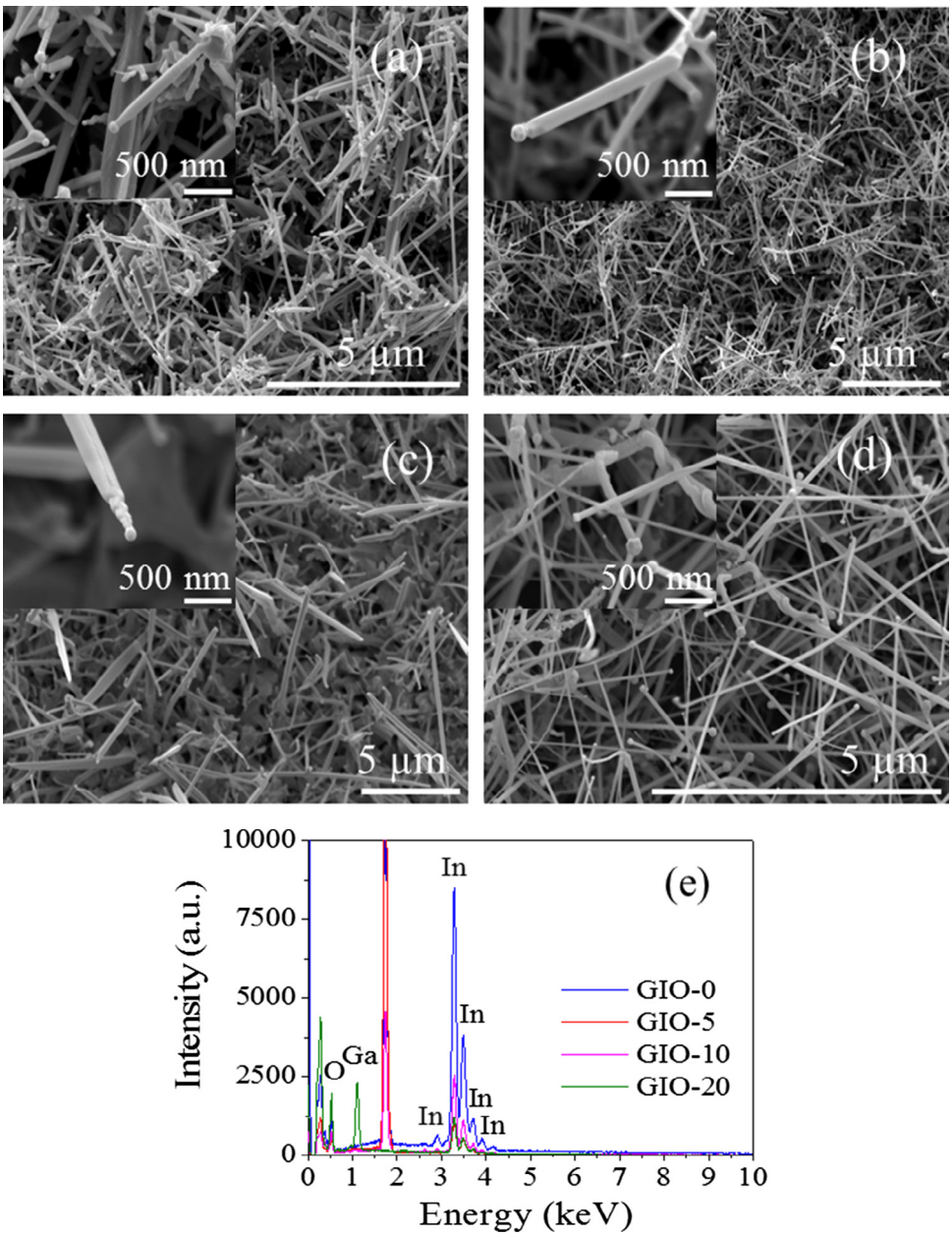

Fig. 1. Typical SEM images of the (a) GIO-0, (b) GIO-5, (c) GIO-10 and (d) GIO-20 samples; and (e) their typical EDS spectra. Amplified images of selected nanostructures (insets) show the presence of Au particles at their tips and their tapered ends.

Quantitative EDS analysis (Fig. 1f and Table 1) of the samples indicates a gradual increment of Ga content in the nanostructures with the increase of nominal Ga%. The Ga/In atom% ratio increased from 0.04 to 0.08 for the sample GIO-5 to GIO-20. The oxygen atom % in all the samples is higher than the expected stoichiometric value (66.67 atom%), while the estimated Ga/In atom% ratios are lower than their expected values (0.08, 0.16 and 0.32 for the GIO-5, GIO-10 and GIO-20, respectively), probably due to the difference in the evaporation rates of In and Ga due to their different vapor pressures (3.2×10^{-5} atm, and 4.6×10^{-6} atm, at 900 °C, respectively) [21].

XRD patterns of the samples (Fig. 2) revealed sharp and intense diffraction peaks, indicating their good crystallinity. The intense diffraction peaks appeared around 21.58, 30.70, 35.62, 41.90, 45.78, 51.14 and 60.78° could be assigned to In_2O_3 in bcc phase (JCPDS card # 06-0416). Two low intensity peaks appeared around 38.80 and 44.46° for all the samples correspond to Au in fcc phase (JCPDS card # 04-0784), coming from the Au used as catalyst. No diffraction peak related to Ga_2O_3, ternary oxide, or any other impu-

Table 1
EDS estimated elemental composition of the fabricated nanostructures.

Sample	Element	Atomic%	Ga/In
GIO-0	In	31.1	0.000
	O	68.9	
GIO-5	In	30.3	0.040
	O	68.5	
	Ga	1.2	
GIO-10	In	28.9	0.052
	O	69.6	
	Ga	1.5	
GIO-20	In	27.1	0.077
	O	70.8	
	Ga	2.1	

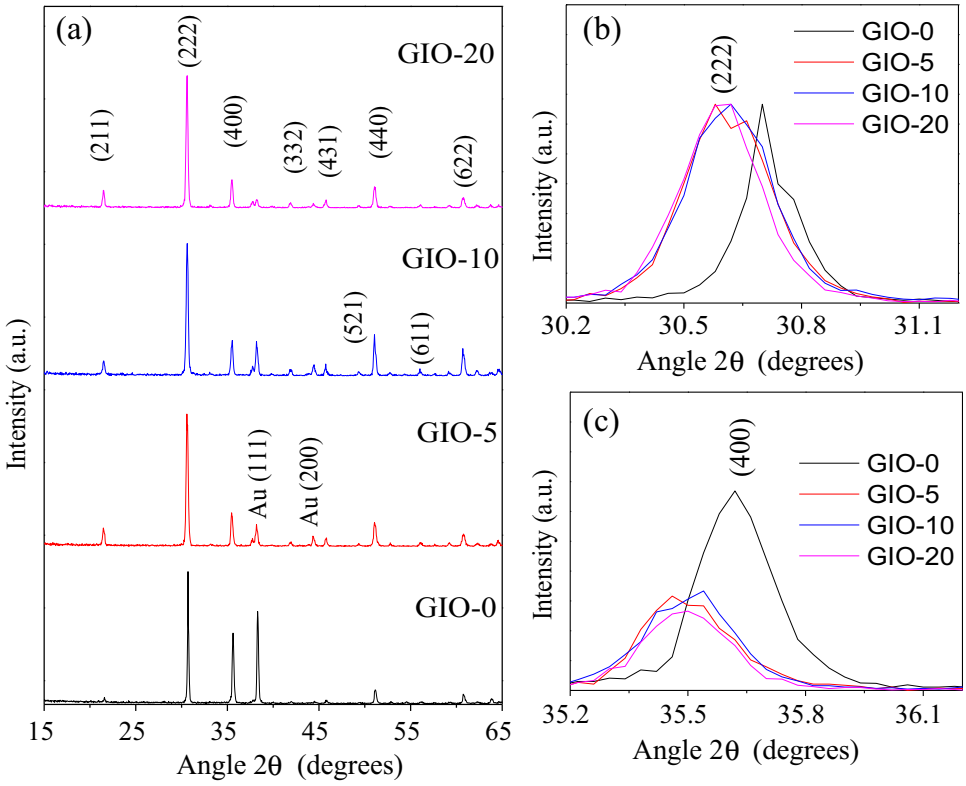

Fig. 2. XRD patterns of the fabricated In_2O_3 nanostructures (a), and their amplified sections showing broadening and shift of the (222) (b) and (400) (c) peaks.

rity could be detected from the XRD spectra of the samples. As can be noticed (Fig. 2), Ga incorporation makes the XRD peaks broader and shifts to lower diffraction angles due to lattice distortion (Fig. 2b and 2c). Since the ionic radii of Ga and In are 0.80 Å and 0.62 Å, respectively [22], the distortion caused by the incorporation of Ga indicates that Ga occupies interstitial sites of the In_2O_3 lattice. However, since the differences in Ga concentration from sample-to-sample were small (Table 1), there was no significat change in the XRD spectra of the samples containing different Ga contents. The lattice parameters $a = b = c$ of the cubic structure ($\alpha = \beta = \gamma = 90°$) were calculated utilizing the equation [23]:

$$d = a/\sqrt{h^2 + k^2 + l^2} \quad (1)$$

where h, k, and l are the Miller indices of the selected peak (plane), and d is the interplanar spacing estimated using Bragg's relation. Estimated lattice parameters of the samples (Table 2) indicate a gradual expansion of unit cell volume on Ga incorporation in In_2O_3 lattice.

Room temperature CL spectra of all the samples revealed a broad emission in the visible range at around 1.75 eV for the pristine In_2O_3 nanostructures, while Ga incorporation causes the appearance of addition emission in the UV region (Fig. 3). Gaussian deconvolution of CL spectra of the samples (Fig. 3b–d) revealed the presence of three component bands centered at ~1.75 (orange), 2.55 (green) and 3.15 eV (violet) in all the Ga-incorporated samples.[1] On Ga incorporation in In_2O_3 nanostructures, the relative intensity of the green band with respect to the orange band (I_g/I_o) increased. The estimated I_g/I_o ratios for the GIO-5, GIO-10, and GIO-20 samples were 0.13, 1.36 and 2.61, respectively. Although the visible emissions in In_2O_3 nanostructures have been frequently

Table 2
Lattice parameters and FWHM of the (222) peak, estimated from the XRD patterns of the grown nanostructures.

Sample	Angle 2θ (°)	Lattice parameter (Å)	FWHM (°)
GIO-0	30.71	10.07	0.19
GIO-5	30.61	10.10	0.25
GIO-10	30.61	10.10	0.25
GIO-20	30.59	10.11	0.26

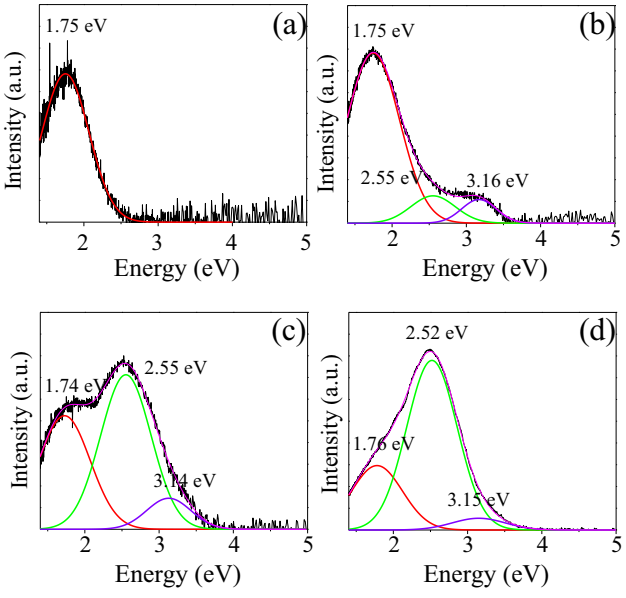

Fig. 3. Deconvoluted CL spectra of (a) GIO-0, (b) GIO-5, (c) GIO-10, and (d) GIO-20 samples showing the evolution of different emissions.

[1] For interpretation of color in Figs. 3 and 6, the reader is referred to the web version of this article.

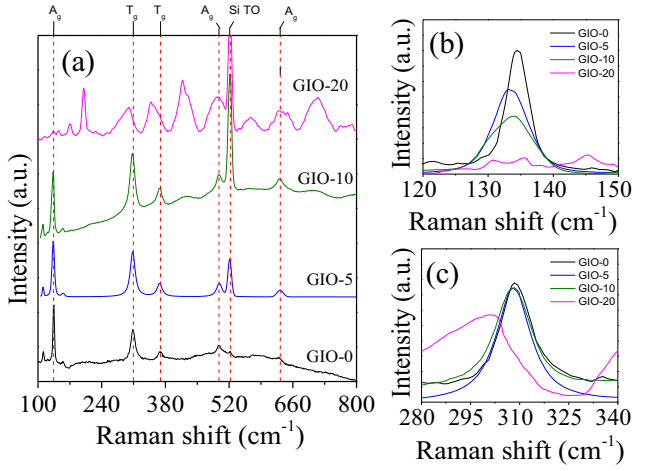

Fig. 4. (a) Raman spectra of the pristine and Ga-incorporated In_2O_3 nanostructures and amplified Raman spectra of the main vibrational modes at (b) ~133 cm^{-1}, and (c) ~308 cm^{-1}, showing their red-shift and broadening due to Ga incorporation. (For interpretation of the references to colour in this figure legend, the reader is referred to the web version of this article.)

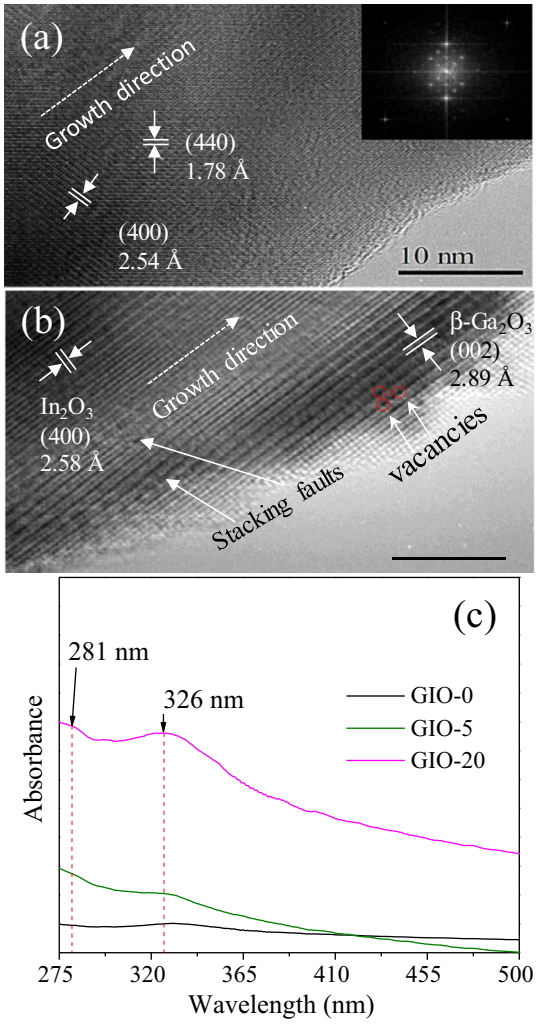

Fig. 5. Typical HRTEM images of a pristine In_2O_3 nanowire and its fast Fourier transform (inset) (a); Ga-incorporated In_2O_3 nanostructure (sample GIO-20) containing different types of point defects (b); UV-vis absorption spectra of the fabricated nanostructures (c).

observed, their origin has been a subject of discussion for several years without a convincing conclusion. Kumar *et al.* [24] have associated the red-orange emission of In_2O_3 appeared around 2.10 eV, to the formation of interstitial In_i^{3+} sites. On the other hand, several authors have associated the green-blue emissions of indium oxide, appearing in between 2.20 and 2.91 eV, to oxygen vacancies [10,18]. Some authors [18,25,26] proposed that the radiative recombination of electrons in ionized oxygen vacancies with photogenerated holes creates V_O-V_{In} pairs in the band gap, inducing the green emission in In_2O_3, similar to ZnO [27]. On Ga incorporation in interstitial sites of In_2O_3 crystal lattice, the relative intensity of the green band increases due to the formation of oxygen-related defects such as V_O. Incorporated Ga can form bonds with the oxygen at the surface of the nanostructures to form GaO_x complexes, increasing the amount of V_O present in the nanostructures, enhancing the green emission. As described by Farvid *et al.* [28] for γ-Ga_2O_3–rh-In_2O_3 nanoparticles, an increment in indium content in gallium oxide causes a narrowing of the band gap of gallium oxide due to the incorporation of In^{3+} in octahedral sites of the spinel-type crystal structure of γ-Ga_2O_3. The substitution of Ga^{3+} by In^{3+} causes a red shift of the emission band of gallium oxide nanostructures. A similar behavior has been found for In-doped gallium oxide micro-/nanostructures grown by thermal treatment [26]. Thus, in the opposite situation, when Ga^{3+} is the foreign cation and indium oxide is the host lattice, a broadening in the band gap of indium oxide occurs due to gallium incorporation, increasing the energy of visible emissions, as seen in the CL spectra of the fabricated Ga-incorporated In_2O_3 nanostructures in the present study. The band appeared around 3.15 eV, which did not appear in pristine In_2O_3 nanostructures can be assigned to the formation of GaO_x containing high concentration of oxygen vacancies. As has been reported by Al-Kuhaili *et al.* [29], in non-stoichiometric gallium oxide, oxygen vacancies form a defect band just below the conduction band, reducing its bandgap. Therefore, the 3.15 eV emission band can be associated to the transition from this donor level to the valence band of In_2O_3. As can be noticed, the intensity of this emission increases with the increase of Ga content in the nanostructures.

Room temperature Raman spectra were measured to analyze the effect of Ga incorporation on the crystallinity and lattice deformation of In_2O_3 nanostructures in 100–800 cm^{-1} spectral range, utilizing a 100x objective lens with a laser beam spot size ~4 μm, focused on different 1D structures (Fig. 4). The vibrational modes detected at 111 ($T_g^{(1)}$), 133 ($A_g^{(1)}$), 153 ($A_g^{(2)}$), 307 ($T_g{}^{(2)}$), 367 ($T_g^{(3)}$), 497 ($A_g^{(3)}$) y 629 cm^{-1} ($A_g^{(4)}$) correspond to the bcc phase of indium oxide (space group I_a^3) [30]. The band appeared around

Table 3
Position and FHWM of the main vibrational modes of pristine and Ga-incorporated In_2O_3.

	Position (FWHM) [cm^{-1}]				
Sample	A_g	T_g	T_g	A_g	A_g
GIO-0	134 (3.80)	309 (11.19)	369 (15.27)	498 (9.99)	628 (27.28)
GIO-5	133 (5.59)	308 (12.42)	367 (13.30)	498 (11.67)	632 (12.41)
GIO-10	129 (3.9)	302 (12.9)	362 (14.1)	494 (23.0)	626 (23.5)
GIO-20	130 (11.44)	300 (15.54)	361 (17.82)	492 (29.23)	634 (32.59)

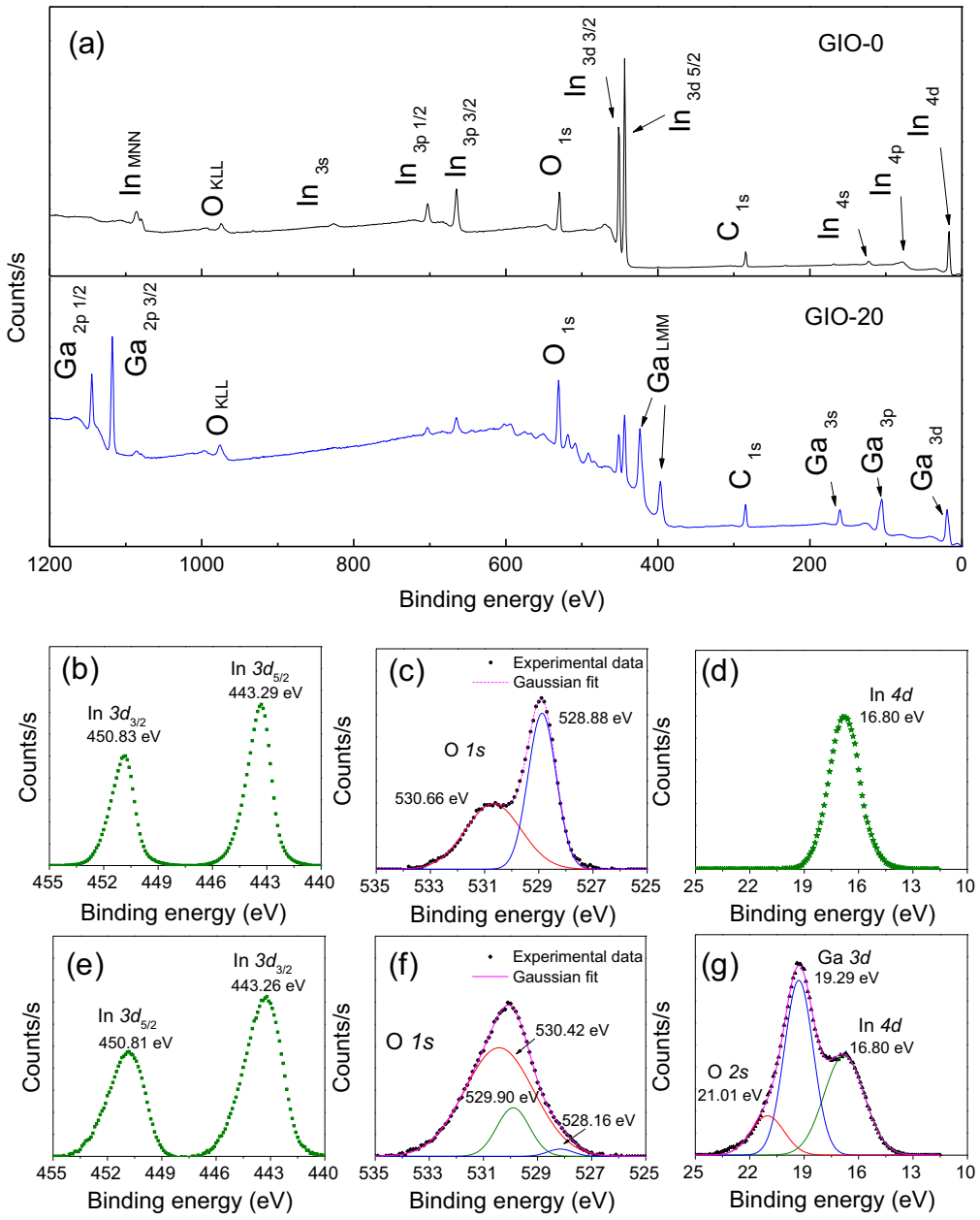

Fig. 6. (a) XPS survey spectra of the pristine and Ga-incorporated In_2O_3 (GIO-20) nanostructures; (b–d) core level In *3d*, O *1s* and In *4d* spectra of the pristine, and (e–g) core level In *3d*, O *1s* and Ga *3d* spectra of the GIO-20 samples. From (d) and (g), the absence of Ga in the pristine sample and the appearance of Ga *3d* peak in Ga-incorporates sample (GIO-20) can be noticed.

133 cm^{-1}, corresponds to the vibrations of In—O bond in the octahedrally-coordinated InO_6 units [31], while the band appeared around 307 cm^{-1} is attributed to bending vibrations of InO_6 units and 367 cm^{-1} band is attributed to the stretching vibrations of the In—O—In bonds. The bands appeared around 497 and 629 cm^{-1} are the stretching vibrations of InO_6 units [32]. Raman spectra of the Ga-incorporated samples reveal the all the vibrational modes of the pristine sample, indicating that the main contribution comes from the In_2O_3 host lattice. On Ga doping, the main vibrational modes, especially those at around 133 and 307 cm^{-1}, become broader and shift to lower energy (Fig. 4b and c, Table 3.). The shift is probably due to the reduction of In—O bond energy as the result of Ga^{3+} substitution at, In^{3+} sites, as observed by Singhal *et al.* [33] in Fe-doped In_2O_3 thin films. For the GIO-20 sample, the vibrational modes are broader and less intense, besides the appearance of additional modes around 175, 204, 420, 564, and 707 cm^{-1}. Although the vibrational modes at 420, 564 and 701 cm^{-1} are rarely observed in Raman spectra of In_2O_3 nanostructures, they have been associated to the bcc phase of In_2O_3 [10,34], while the modes at 175 and 204 cm^{-1} have been assigned to β-Ga_2O_3 [26,35] and correspond to libration/translation vibrations of the tetrahedral-octahedral structural units chains [35]. The appearance of vibrational modes associated to gallium oxide might have been caused by the segregation of Ga in some parts of the nanowires forming Ga_2O_3 or GaO_x crystallites or agglomerates, similar to the segregation of In impurities in In-doped gallium oxide micro-/nanostructures, observed by López *et al.* [26].

Effect of Ga incorporation on the crystallinity and defect structure of the nanostructures were studied further using transmission electron microscopy (TEM). High-resolution TEM (HRTEM) images of the pristine nanostructures (Fig. 5a) revealed their high crystalline quality, grown preferably along [400] direction, maintaining

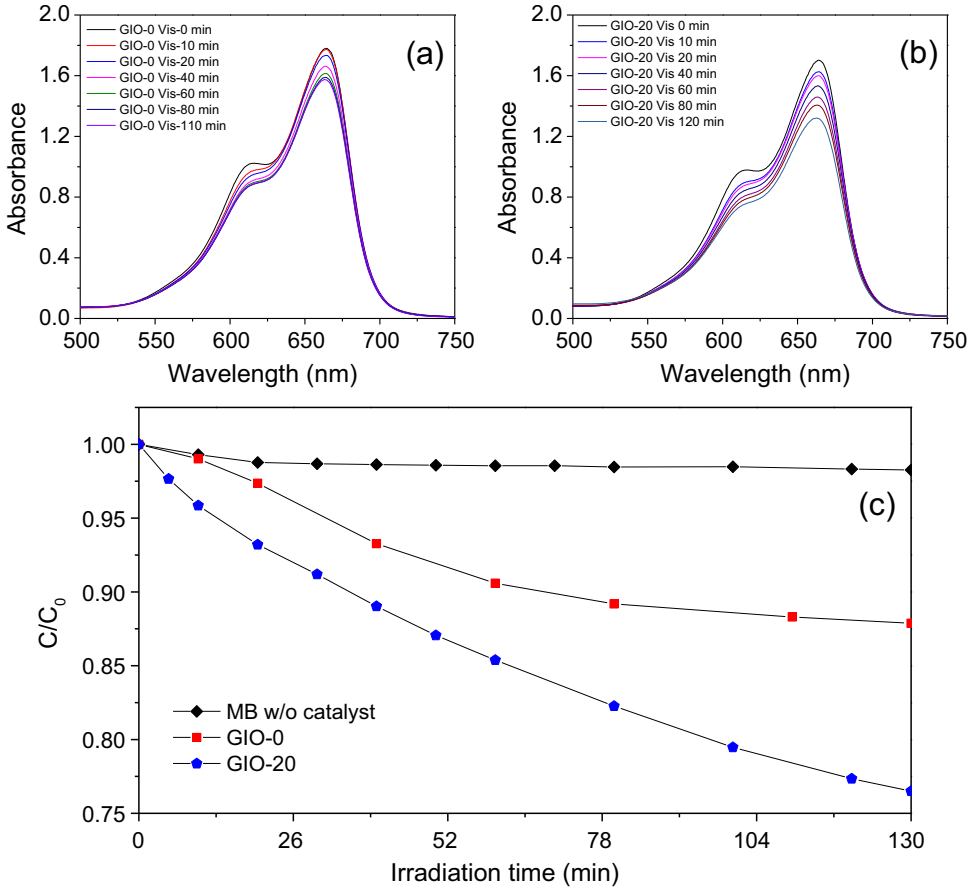

Fig. 7. MB absorption spectra of the (a) GIO-0 and (b) GIO-20 samples, and (c) C/C_0 vs irradiation time plots showing their degradation performance. The MB degradation behavior under visible light illumination has also been included in (c) to show that there is no photo-degradation of MB in absence of catalyst.

interplanar spacing (2.54 Å) close to the standard one (2.52 Å). However, on Ga incorporation (Fig. 5b), the interplanar spacing increased, demonstrating an expansion of In_2O_3 lattice due to the accumulation of Ga at interstitial spaces, in agreement with the obtained XRD results. A rigorous inspection of HRTEM images of Ga-incorporated nanostructures revealed the presence of gallium oxide clusters, which supports the results obtained from their CL and Raman studies. In the Ga-incorporated sample, apart from the formation of gallium oxide agglomerates, which are mainly accumulated near the surface of the nanowires due to the low solubility of gallium oxide in indium oxide [15], several other defects such as vacancies, and stacking faults are observed.

Room temperature absorption spectra (Fig. 5c) of the nanostructures were recorded in UV–Vis (270–700 nm) spectral range to monitor the change in their optical properties on Ga incorporation. Absorption spectrum of the pristine sample revealed an absorption band around 330 nm (3.75 eV), associated to the near band edge absorption of In_2O_3. On Ga incorporation, the absorption peak shifted towards lower wavelength by about 4 nm, probably due to the strain induced by Ga incorporation at interstitial sites. The shift is almost equal for all the Ga-incorporated samples, as there was no significant variation in Ga content in them (Table 1). There appeared an additional weak absorption band around 281 nm (4.41 eV) for the Ga-incorporated samples. The energy position of this absorption band is substantially higher than the reported band gap values of In_2O_3, but relatively close to the band gap energy of Ga_2O_3 (4.8 eV) [26]. As has been reported by Gowtham *et al.* [36], the calculated band gap of GaO_x clusters ($0.3 < x < 3$) vary from 1.55 to 2.71 eV, and from 2.53 to 4.92 eV for neutral and positively charged clusters. Hence, the incorporation of Ga in interstitial sites of In_2O_3 lattice can induce the formation of gallium oxides (GaO_x) clusters at the surface of their 1D structures, which are responsible for the absorption band at 281 nm.

To verify the presence of partially oxidized Ga in the Ga-incorporated In_2O_3 nanostructures, we performed XPS analysis on the pristine GIO-0 and nominal 20% Ga-incorporates GIO-20 samples. While the XPS survey spectrum of the pristine sample revealed the presence of In and O, the survey spectrum of the GIO-20 samples revealed the presence of Ga, apart from In and O. The core-level spectra of In, O, and Ga, recorded in their respective emission energy range, are presented in Fig. 6(b–g) for the pristine and Ga-incorporated nanostructures, respectively. The deconvoluted core-level O *1s* emission of the pristine sample (Fig. 6c) revealed two component bands around 528.87 and 530.66 eV, corresponding to oxygen in indium oxide and adsorbed oxygen in the nanorod surface. On the other hand, the deconvoluted O *1s* emission of the GIO-20 sample (Fig. 6f) revealed three components along with a small red shift of the oxide-related band (In—O bond in In_2O_3), indicating a change in chemical environment of In in the Ga-impurified nanostructures. Appearance of the 529.90 eV component clearly indicates the formation of oxide bond with another element apart from indium.

A deconvolution of the Ga *3d* emission band of the GIO-20 sample (Fig. 6 g) revealed three component bands appearing around 16.80, 19.29 and 21.01 eV, which correspond to the core level emissions of In *4d*, Ga *3d* and O *2s* bands, respectively [37]. Typically, the binding energy of Ga *3d* level is around 20.6 eV in gallium oxide, while the binding energy for elemental Ga is around 18.5 eV. However, in

the core-level spectrum of GIO-20 sample in Ga *3d* region, the binding energy of Ga *3d* is shifted slightly to lower energy (19.29 eV), indicating the formation of gallium sub-oxides, such as Ga_2^+O species due to incomplete oxidation of gallium [38].

To study the effect of Ga incorporation and hence the formation of additional defect levels in the band gap of In_2O_3 nanostructures on their photocatalytic performance, GIO-0 and GIO-20 samples were tested for MB degradation both under ultraviolet and visible light. While none of these samples revealed any significant response under ultraviolet irradiation (365 nm), they manifested reasonable photocatalytic performance under visible light (Fig. 7). The mechanism of defect-induced photocatalytic degradation of organic dyes by metal oxide nanostructures has been discussed in our earlier works [39,19]. As can be noticed (Fig. 7), the MB degradation efficiency of the In_2O_3 nanostructures increased drastically (~94%) after Ga-incorporation. The enhanced photocatalytic activity of the Ga-incorporated nanostructures is probably associated to the presence of defect levels in high concentration in their electronic band gap, which act as trapping levels of photo-generated electrons, prohibiting them to recombine with holes at the valence band.

4. Conclusions

In summary, we present the fabrication of Ga-incorporated 1D In_2O_3 nanostructures of several micrometer length and tens to hundreds of nanometer width through VLS growth process. The pure In_2O_3 nanostructures are strain relaxed, highly crystalline, containing structural defects in lower concentrations. Ga incorporation at the interstitial sites of the In_2O_3 nanostructures, especially above 1.0 atom%, strongly affects their morphology, induces a lattice expansion, and several shallow defect levels in their optical band gap. Incorporation of Ga atoms in excess at the interstitial sites of In_2O_3 lattice induces the formation of GaO_x clusters, affecting the absorption and emission behavior of the host matrix severely. Moreover, Ga incorporation at the interstitial sites of In_2O_3 nanostructures extends their defect-induced luminescence emission towards visible spectral range, extending the possibility of their applications in visible photocatalytic reactions and other optoelectronic applications.

Acknowledgements

The work was partially supported by VIEP-BUAP, Mexico (Grant # VIEP/EXC/2017-257). JARR thanks CONACyT, Mexico for extending doctoral fellowship (# 290840). The authors are grateful to Dr. S. Shaji, Facultad de Ingeniería Mecánica y Eléctrica, Universidad Autónoma de Nuevo León, for his help in the XPS analysis of the nanostructures.

References

[1] V.P. Reddy, A.V. Kumar, K. Swapna, K.R. Rao, Nano indium oxide as a recyclable catalyst for C-S cross-coupling of thiols with aryl halides under ligand free conditions, Org. Lett. 11 (2009) 1697–1700, https://doi.org/10.1021/ol900009a.
[2] T. Bielz, H. Lorenz, P. Amann, B. Klötzer, S. Penner, Water-gas shift and formaldehyde reforming activity determined by defect chemistry of polycrystalline In_2O_3, J. Phys. Chem. C 115 (2011) 6622–6628, https://doi.org/10.1021/jp111739m.
[3] M. Kumar, V.N. Singh, B.R. Mehta, J.P. Singh, Tunable growth of indium oxide from nanoflute to metal-filled nanotubes, J. Phys. Chem. C 116 (2012) 5450–5455, https://doi.org/10.1021/jp211658a.
[4] D. Zhang, C. Li, S. Han, X. Liu, T. Tang, W. Jin, C. Zhou, Electronic transport studies of single-crystalline In_2O_3 nanowires, Appl. Phys. Lett. 82 (2003) 112–114, https://doi.org/10.1063/1.1534938.
[5] Y. Kokubun, T. Abe, S. Nakagomi, Sol-gel prepared $(Ga_{1-x}In_x)_2O_3$ thin films for solar-blind ultraviolet photodetectors, Phys. Status Solidi Appl. Mater. Sci. 207 (2010) 1741–1745, https://doi.org/10.1002/pssa.200983712.
[6] V.D. Das, S. Kirupavathy, L. Damodare, N. Lakshminarayan, Optical and electrical investigations of indium oxide thin films prepared by thermal oxidation of indium thin films, J. Appl. Phys. 79 (1996) 8521–8530, https://doi.org/10.1063/1.362477.
[7] S. Ju, F. Ishikawa, P. Chen, H.-K. Chang, C. Zhou, Y. Ha, J. Liu, A. Facchetti, T.J. Marks, D.B. Janes, High performance In_2O_3 nanowire transistors using organic gate nanodielectrics, Appl. Phys. Lett. 92 (2008) 222105, https://doi.org/10.1063/1.2937111.
[8] M. Kumar, B.R. Mehta, V.N. Singh, R. Chatterjee, S. Milikisiyants, K.V. Lakshmi, J. P. Singh, The role of stoichiometry of indium and oxygen on gas sensing properties of indium oxide nanostructures, Appl. Phys. Lett. 96 (2010) 148–151, https://doi.org/10.1063/1.3371717.
[9] M. Mazzera, M. Zha, D. Calestani, A. Zappettini, L. Lazzarini, G. Salviati, L. Zanotti, Low-temperature In_2O_3 nanowire luminescence properties as a function of oxidizing thermal treatments, Nanotechnology 18 (2007) 355707, https://doi.org/10.1088/0957-4484/18/35/355707.
[10] D. León Sanchez, J.A. Ramos Ramón, M. Herrera Zaldívar, U. Pal, E. Rubio Rosas, Structure and optical properties of vapor grown In_2O_3:Ga nano-/microcrystals, Adv. Nano Res. 3 (2015) 81–96, https://doi.org/10.12989/anr.2015.3.2.081.
[11] Y. Yan, Y. Zhang, H. Zeng, J. Zhang, X. Cao, L. Zhang, Tunable synthesis of In_2O_3 nanowires, nanoarrows and nanorods, Nanotechnology 18 (2007) 175601, https://doi.org/10.1088/0957-4484/18/17/175601.
[12] P. Gali, G. Sapkota, A.J. Syllaios, C. Littler, U. Philipose, Stoichiometry dependent electron transport and gas sensing properties of indium oxide nanowires, Nanotechnology 24 (2013) 225704, https://doi.org/10.1088/0957-4484/24/22/225704.
[13] O. Mryasov, A. Freeman, Electronic band structure of indium tin oxide and criteria for transparent conducting behavior, Phys. Rev. B 64 (2001) 233111, https://doi.org/10.1103/PhysRevB.64.233111.
[14] J.M. Phillips, R.J. Cava, G.A. Thomas, S.A. Carter, J. Kwo, T. Siegrist, J.J. Krajewski, J.H. Marshall, W.F. Peck, D.H. Rapkine, Zinc-indium-oxide: a high conductivity transparent conducting oxide, Appl. Phys. Lett. 67 (1995) 2246–2248, https://doi.org/10.1063/1.115118.
[15] H.J. Chun, Y.S. Choi, S.Y. Bae, H.C. Choi, J. Park, Single-crystalline gallium-doped indium oxide nanowires, Appl. Phys. Lett. 85 (2004) 461–464, https://doi.org/10.1063/1.1771816.
[16] J.M. Phillips, J. Kwo, G.A. Thomas, S.A. Carter, R.J. Cava, S.Y. Hou, J.J. Krajewski, J. H. Marshall, W.F. Peck, D.H. Rapkine, R.B. van Dover, Transparent conducting thin films of $GaInO_3$, Appl. Phys. Lett. 65 (1994) 115–117, https://doi.org/10.1063/1.113052.
[17] W. Zhang, J. Jie, Z. He, S. Tao, X. Fan, Y. Zhou, G. Yuan, L. Luo, W. Zhang, C.S. Lee, S.T. Lee, Single zinc-doped indium oxide nanowire as driving transistor for organic light-emitting diode, Appl. Phys. Lett. 92 (2008) 1–4, https://doi.org/10.1063/1.2909716.
[18] J. Gao, R. Chen, D.H. Li, L. Jiang, J.C. Ye, X.C. Ma, X.D. Chen, Q.H. Xiong, H.D. Sun, T. Wu, UV light emitting transparent conducting tin-doped indium oxide (ITO) nanowires, Nanotechnology 22 (2011) 195706, https://doi.org/10.1088/0957-4484/22/19/195706.
[19] R. Sánchez Zeferino, J.A. Ramos Ramón, M.E. De Anda Reyes, R. Silva Gónzalez, U. Pal, Large scale synthesis of ZnO nanostructures of different morphologies through solvent-free mechanochemical synthesis and their application in photocatalytic dye degradation, Am. J. Eng. Appl. Sci. (2015), https://doi.org/10.3844/ajeassp.2016.41.52.
[20] J. Ba, D.F. Rohlfing, A. Feldhoff, T. Brezesinski, I. Djerdj, M. Wark, M. Niederberger, Nonaqueous synthesis of uniform indium tin oxide nanocrystals and their electrical conductivity in dependence of the tin oxide concentration, Chem. Mater. 18 (2006) 2848–2854, https://doi.org/10.1021/cm060548q.
[21] R.E. Honig, Vapor pressure data for the more common elements, RCA Rev. A Tech. J. 18 (1957) 195–204.
[22] R.D. Shannon, Revised effective ionic radii and systematic studies of interatomic distances in halides and chalcogenides, Acta Crystallogr. Sect. A 32 (1976) 751–767, https://doi.org/10.1107/S0567739476001551.
[23] M. Jothibas, C. Manoharan, S. Johnson Jeyakumar, P. Praveen, Study on structural and optical behaviors of In_2O_3 nanocrystals as potential candidate for optoelectronic devices, J. Mater. Sci. Mater. Electron. 26 (2015) 9600–9606, https://doi.org/10.1007/s10854-015-3623-x.
[24] M. Kumar, V.N. Singh, F. Singh, K.V. Lakshmi, B.R. Mehta, J.P. Singh, On the origin of photoluminescence in indium oxide octahedron structures, Appl. Phys. Lett. 92 (2008) 171907, https://doi.org/10.1063/1.2910501.
[25] T. Gao, T. Wang, Catalytic growth of In_2O_3 nanobelts by vapor transport, J. Cryst. Growth 290 (2006) 660–664, https://doi.org/10.1016/j.jcrysgro.2006.01.046.
[26] I. López, A.D. Utrilla, E. Nogales, B. Méndez, J. Piqueras, A. Peche, J. Ramírez-Castellanos, J.M. González-Calbet, In-doped gallium oxide micro- and nanostructures: morphology, structure, and luminescence properties, J. Phys. Chem. C 116 (2012) 3935–3943, https://doi.org/10.1021/jp210233p.
[27] K. Vanheusden, W.L. Warren, C.H. Seager, D.R. Tallant, J.A. Voigt, B.E. Gnade, Mechanisms behind green photoluminescence in ZnO phosphor powders, J. Appl. Phys. 79 (1996) 7983–7990, https://doi.org/10.1063/1.362349.
[28] S.S. Farvid, T. Wang, P.V. Radovanovic, Colloidal gallium indium oxide nanocrystals: a multifunctional light-emitting phosphor broadly tunable by alloy composition, J. Am. Chem. Soc. 133 (2011) 6711–6719, https://doi.org/10.1021/ja111514u.
[29] M.F. Al-Kuhaili, S.M.A. Durrani, E.E. Khawaja, Optical properties of gallium oxide films deposited by electron-beam evaporation, Appl. Phys. Lett. 83 (2003) 4533–4535, https://doi.org/10.1063/1.1630845.

[30] C. Kranert, R. Schmidt-Grund, M. Grundmann, Raman active phonon modes of cubic In_2O_3, Phys. Status Solidi - Rapid Res. Lett. 8 (2014) 554–559, https://doi.org/10.1002/pssr.201409004.
[31] X. Wang, Z. Chen, K. Saito, T. Tanaka, M. Nishio, Q. Guo, Temperature-dependent Raman scattering in cubic $(InGa)_2O_3$ thin films, J. Alloys Compd. 690 (2017) 287–292, https://doi.org/10.1016/j.jallcom.2016.08.129.
[32] S. Sänze, A. Gurlo, C. Hess, Monitoring gas sensors at work: operando Raman-FTIR study of ethanol detection by indium oxide, Angew. Chem. - Int. Ed. 52 (2013) 3607–3610, https://doi.org/10.1002/anie.201207258.
[33] A. Singhal, S.N. Achary, J. Manjanna, O.D. Jayakumar, R.M. Kadam, A.K. Tyagi, Colloidal Fe-doped indium oxide nanoparticles: facile synthesis, structural, and magnetic properties, J. Phys. Chem. C 113 (2009) 3600–3606, https://doi.org/10.1021/jp8097846.
[34] D.-W. Kim, I.-S. Hwang, S.J. Kwon, H.-Y. Kang, K.-S. Park, Y.-J. Choi, K.-J. Choi, J.-G. Park, Highly conductive coaxial SnO_2–In_2O_3 heterostructured nanowires for Li ion battery electrodes, Nano Lett. 7 (2007) 3041–3045, https://doi.org/10.1021/nl0715037.
[35] R. Rao, A.M. Rao, B. Xu, J. Dong, S. Sharma, M.K. Sunkara, Blueshifted Raman scattering and its correlation with the [110] growth direction in gallium oxide nanowires, J. Appl. Phys. 98 (2005) 94312, https://doi.org/10.1063/1.2128044.
[36] S. Gowtham, M. Deshpande, A. Costales, R. Pandey, Structural, energetic, electronic, bonding, and vibrational properties of Ga_3O, Ga_3O_2, Ga_3O_3, Ga_2O_3, and GaO_3 Clusters, J. Phys. Chem. B 109 (2005) 14836–14844, https://doi.org/10.1021/jp050801u.
[37] R. Carli, C.L. Bianchi, XPS analysis of gallium oxides, Appl. Surf. Sci. 74 (1994) 99–102, https://doi.org/10.1016/0169-4332(94)90104-X.
[38] B. Zheng, W. Hua, Y. Yue, Z. Gao, Dehydrogenation of propane to propene over different polymorphs of gallium oxide, J. Catal. 232 (2005) 143–151, https://doi.org/10.1016/j.jcat.2005.03.001.
[39] M.D.L. Ruiz Peralta, U. Pal, R.S. Zeferino, Photoluminescence (PL) quenching and enhanced photocatalytic activity of Au-decorated ZnO nanorods fabricated through microwave-assisted chemical synthesis, ACS Appl. Mater. Interf. 4 (2012) 4807–4816, https://doi.org/10.1021/am301155u.